ELSEVIER

Biophysical Chemistry 53 (1995) 259–266

Biophysical Chemistry

Solution X-ray scattering study on the chaperonin GroEL from *Escherichia coli*

Yoshihiko Igarashi [a,*], Kazumoto Kimura [b], Kaoru Ichimura [a], Shigeru Matsuzaki [a], Teikichi Ikura [c], Kunihiro Kuwajima [c], Hiroshi Kihara [d]

[a] *Department of Biochemistry, Dokkyo University School of Medicine, Mibu, Tochigi 321-02, Japan*
[b] *Division of Medical Electronics, Dokkyo University School of Medicine, Mibu, Tochigi 321-02, Japan*
[c] *Department of Physics, School of Science, University of Tokyo, Bunkyo 113, Japan*
[d] *Physics Laboratory, Kansai Medical University, Hirakata 573, Japan*

Received 9 June 1994; accepted in revised form 29 August 1994

Abstract

The molecular architecture of native GroEL has been studied by solution X-ray scattering. The radius of gyration for the native molecule was estimated to be 66.0 Å in 50 mM Tris–HCl, 100 mM KCl at pH 7.5 and 25°C. The maximum dimension was estimated to be 170 Å, based on the pair distance distribution function. A cylindrical structure or two heptameric rings was found to be the best for native GroEL among structures examined by using a multi-sphere model analysis in which the radius of constituent sphere was 6 Å. The results of the model analysis show that the radius of GroEL is 68.0 Å and the height is 150.7 Å. Unexpectedly, the central penetrating hole through GroEL was not confirmed in the best-fit structure.

Keywords: Molecular chaperone; GroEL; Escherichia coli; Model analysis; Solution X-ray scattering

1. Introduction

Folding and assembly of proteins may not always proceed spontaneously in a biological cell but are facilitated by various protein factors including those known as molecular chaperones. The chaperonin GroEL from *E. coli* is one of the best characterized chaperone proteins and consists of 14 equal subunits whose molecular mass is 57.3 kDa as calculated from the amino acid sequence [1]. Refolding reactions of rhodanese, dihydrofolate reductase [2,3] and some other proteins are known to be promoted by GroEL with ATP hydrolysis in the presence of Mg^{2+}, K^+ and GroES by preventing formation of nonspecific insoluble aggregates. Electron microscopic studies have shown that the molecular structure of GroEL is of 7-fold symmetry and consists of 14 subunits which are arranged in two stacked heptameric rings [4–7]. The central space of the ring structure, forming a hole or channel, has been shown to have a diameter of approximately 60 Å [7].

Since the molecular structure of GroEL has been studied in desiccated forms, it is important to elucidate its structure in solution. The technique of solu-

* Corresponding author. Tel.: (+81-282)872127, fax.: (+81-282)865678.

0301-4622/95/$09.50
SSDI 0301-4622(94)00107-3

tion X-ray scattering has proven to be a useful tool for gaining information on the gross conformation for macromolecules in solution [8]. There is, however, only a preliminary structural report by X-ray crystallography of *E. coli* GroEL by Spangfort et al. [9]. The present study deals with the GroEL structure in solution as analyzed by solution X-ray scattering.

2. Materials and methods

2.1. Purification of GroEL from E. coli

A plasmid pKY206 containing a wild type GroE operon from *E. coli* was kindly supplied by Professor K. Ito, Institute for Virus Research, Kyoto University [10].

The GroEL was purified by overexpressing *E. coli* TG1 bearing the plasmid according to the published procedure [11,12] with slight modifications. Briefly, crude GroEL was prepared from soluble lysate by precipitation between 30 and 50% ammonium sulfate saturation. The precipitates were resuspended in an equal volume of 50 mM Tris–HCl containing 1 mM dithiothreitol and 1 mM EDTA at pH 7.5 and 4°C and then fractionated by Sephacryl S-300HR gel chromatography. The GroEL peak was identified by ATP hydrolysis activity [2,13] and by molecular mass (ca. 60 kDa) determined on SDS-PAGE. The GroEL containing fractions were pooled and then loaded onto a DEAE Sepharose FF ion-exchange column equilibrated with the same Tris buffer. After washing with a three column volume of the same buffer, GroEL was eluted from the column with a linear salt gradient of 0 to 0.5 M KCl. Pooled fractions of native GroEL were dialyzed against 50 mM Tris–HCl containing 100 mM KCl at pH 7.5 and 4°C. Homogeneity of GroEL preparations was judged by the SDS-PAGE analysis [14].

Protein concentration of GroEL was determined spectrophotometrically using the absorbance value of $A_{280\ nm}$ (0.1%, 1 cm) = 0.25 [3].

2.2. Solution X-ray scattering study

X-ray scattering analyses were performed at the beam line 15A of the Photon Factory, National Laboratory for High Energy Physics as described

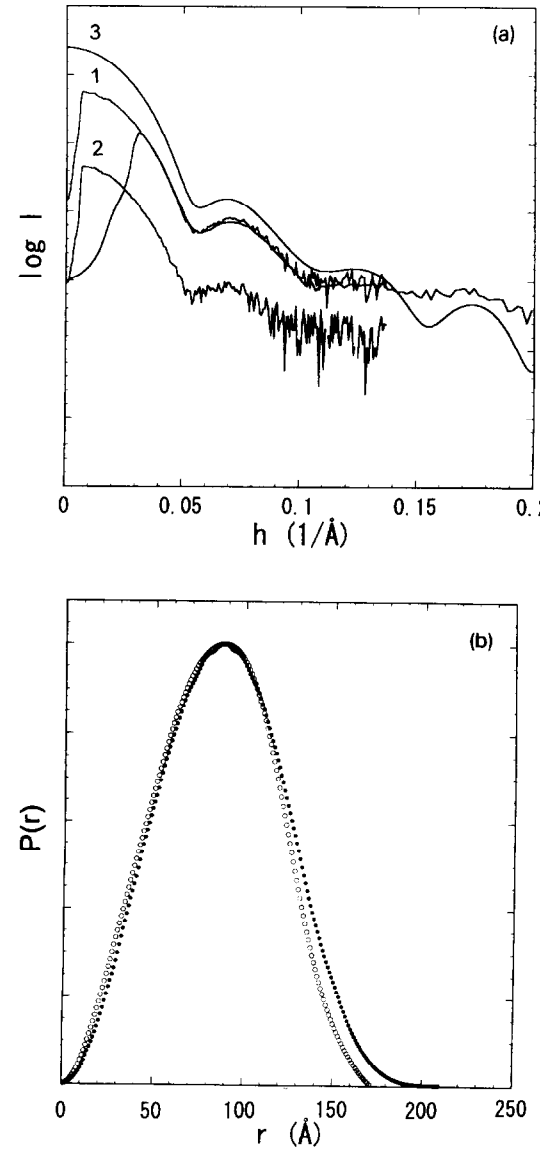

Fig. 1. (a) 1: The composite X-ray scattering curve of 1.2% GroEL observed by long and short camera. 2: The X-ray scattering curve at zero GroEL concentration were obtained by extrapolating of the observed scattering curves at 1.2, 0.9, 0.45 and 0.225% GroEL. 3: The simulated curve calculated from the cylinder model (1766 unit spheres). $\lambda = 1.504$ Å; exposure time, 300 s; camera length 2318 mm for the long camera and 750 mm for the short camera; intensity is normalized to a ring current of 100 mA. The vertical axis is arbitrary unit. (b) The $P(r)$ function of GroEL calculated from the experimental data (open circle) and the simulated curve of the cylinder model (closed circle).

previously [15,16]. Samples in a quartz cell with 1 mm path length were irradiated with monochromatic X-ray (1.504 Å) and the temperature of the cell holder was kept at 25.0°C by circulating water. The X-ray scattering curve of GroEL was measured at two different camera lengths, a long-camera length, $l = 2318$ mm, for molecular mass measurement and a short-camera length, $l = 750$ mm, for molecular internal information. The exposure time was 300 s for each sample. When the scattering curves of GroEL were measured for 30, 60, 300 and 600 s, essentially the same results were obtained. Scattered X-ray patterns were measured at 1.2, 0.9, 0.45 and 0.225% of GroEL concentration, respectively. Scattered X-ray intensities were recorded on a position-sensitive proportional counter (512 channels) with a channel width of 0.368 mm. X-ray scattering data were expressed in terms of $h = 4\pi \sin \theta/\lambda$ (λ, wavelength; 2θ, scattering angle). To inspect the molecular architecture of GroEL in solution, multi-sphere model analyses [17,18] were carried out using the program developed by Sato and co-workers [19].

3. Results and discussion

3.1. Solution X-ray scattering

Solution X-ray scattering of native GroEL was measured in 50 mM Tris–HCl buffer containing 100 mM KCl at pH 7.5 and 25°C. The line 1 in Fig. 1a shows a composite scattering curve obtained from long- and short-camera length data. The original scattering curves measured at the different camera lengths overlapped with each other from the first shoulder to the third peak. The scattering curve displays two major minima at $h = 0.06$ and 0.105 $Å^{-1}$ and one faint minimum at $h = 0.15$ $Å^{-1}$. None of the troughs were very sharp. Maximum peaks are found at $h = 0$, 0.07 and 0.13 $Å^{-1}$. The last peak at $h = 0.13$ $Å^{-1}$ is not so distinct but present. The line 2 in Fig. 1a shows a X-ray scattering curve of extrapolated to zero concentration in a long camera range (from $h = 0$ to 0.13 $Å^{-1}$). The positions of the troughs and peaks of this curve are coincident with those in the scattering pattern at 1.2% GroEL. The pair distance distribution function, $P(r)$, was evaluated and is shown as open circle in Fig. 1b. The pattern of the $P(r)$ function shows a near symmetrical peak. The peak position of $P(r)$ function was 90 Å. The maximum dimension, which corresponds to the longest length of the intraparticle, was estimated to be 170 Å. The radius of gyration, R_g, of GroEL can be estimated by the Guinier plots of the normalized scattering curve. Considering the effect of the protein concentration on the scattering pattern, however, the R_g value at zero protein concentration should be evaluated. For this purpose, two different

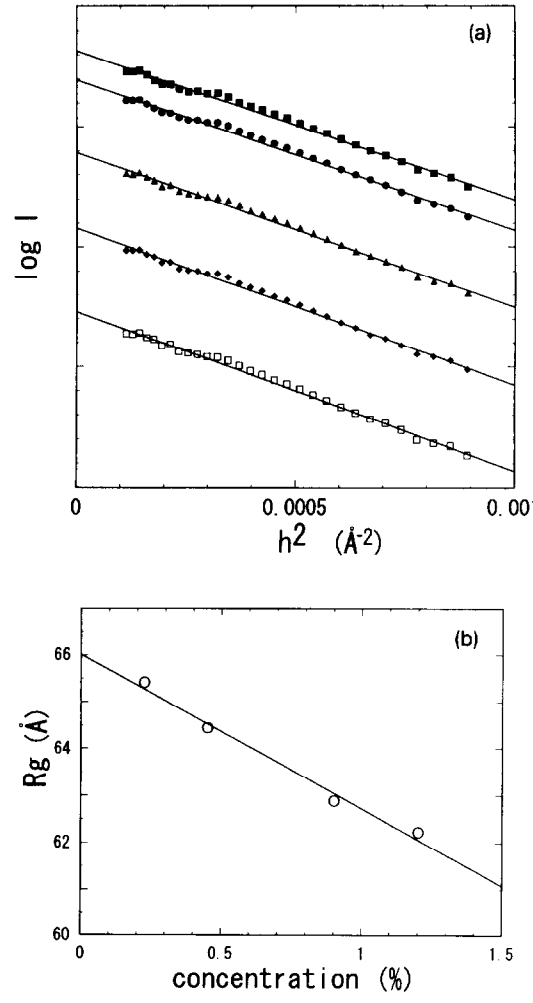

Fig. 2. (a) The Guinier plot at various GroEL concentrations 1.2% (■), 0.9% (●), 0.45% (▲), 0.225% (◆), and the Guinier plot extrapolated to zero protein concentration (□). The vertical axis is arbitrary unit. (b) Concentration dependence of the apparent R_g values obtained from the Guinier plots at different protein concentration.

methods were used to extrapolate the observed R_g values. First, the apparent R_g values were calculated from a series of the Guinier plots at different concentration of GroEL (Fig. 2a). The apparent R_g values thus obtained were linearly extrapolated to zero concentration of GroEL, which gave the R_g of 66.0 ± 0.3 Å (Fig. 2b). Second, the X-ray scattering curves observed at different protein concentrations were directly extrapolated to zero concentration of GroEL. The R_g was then obtained from the Guinier plot of the extrapolated scattering curve and estimated to be 66.0 Å. Thus, both the methods gave the same R_g.

3.2. Model analyses

We used the multi-sphere model analysis [17,18] with a radius of a constituent sphere of 6 Å to obtain the structure best fit to the scattering curve of native GroEL. The size (height or diameter) of model structure shown below corresponds to the center to center distance of the two constituent spheres that are located at both ends of the model structure. In the initial stage of the model simulation, we tried to fit the R_g value of models with that of the GroEL molecule (66.0 ± 0.3 Å). At the first step, three types of models were investigated. The simplest model among them was of sphere type. The radius of the best fit among the models, which was composed of 2038 unit spheres, was 85 Å and the R_g value of this sphere was calculated to be 66.5 Å. The scattering curve of the sphere model showed that all the minima of the curve shifted to the lower h values and were deeper than the experimentally observed minima (data not shown). The second model was an ellipsoid of revolution. When the ratios of long and short axes were set as 1.2(94.4/80), 1.6(109.3/70) and 2(121.6/60), the R_g values were estimated to be 66.0, 66.2 and 66.2 Å, respectively. These values were in close agreement with the experimental data. When the R_g value was kept constant, these sets showed that the length of the long axis was inversely proportional to that of the short axis. However, none of the scattering curves of these models were coincident with the experimental curve (data not shown). The last model was of cylinder type. The candidates of dimension were as follows. The dimension of GroEL structure was first based on the electron micrographs reported by Langer et al. [7], i.e. the

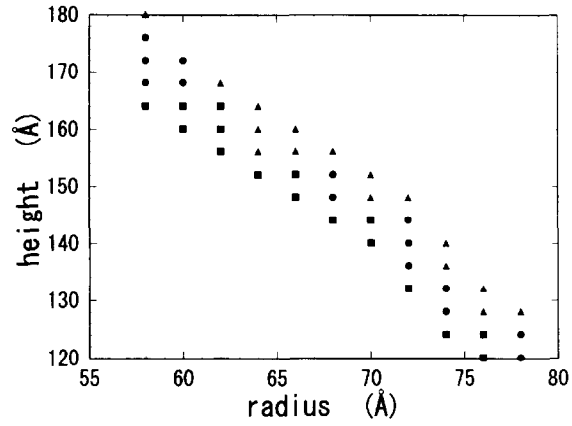

Fig. 3. The relationships among the evaluated R_g, the radius and the height of the cylinder model. (■) Rg < 65.5 Å, (●) 65.5 Å ≤ Rg < 66.5 Å, (▲) 66.5 Å ≤ R_g.

radius was 72.5 Å and the height was 160 Å. The R_gs were calculated for each set with radii varied between 58 and 78 Å and height varied between 120 and 180 Å. The relationships among the evaluated R_g, the radius (r) and the height (h) are shown in Fig. 3 for R_g between 65 and 68 Å, r from 58 to 78 Å, and h from 120 to 180 Å. The R_gs of cylinder models whose dimensions are of r = 68 Å and h = 148–152 Å and of r = 58 Å and h = 168–174 Å are in a range of the experimental R_g value (66.0 ± 0.3 Å). The GroEL model structure that gave the best fit among the structures examined to the observed scattering curve resembles a cylinder with a radius of 68.0 Å and a height of 150.7 Å. This model showed the R_g of 66.2 Å. The simulated scattering curve for the cylinder model structure is depicted by line 3 in Fig. 1a for comparison with that observed experimentally. The simulated curve displays maxima and minima at positions identical to those of the observed curve, indicating a good fit of the model structure. The third minimum of this model showed a deeper trough, but its position coincided with that in the experimental curve. The fourth maxima and further peaks of the model were no more detectable in the experimental curve. The ratio of the first shoulder to the first maximum is nearly the same between the two curves.

The simulated $P(r)$ function (closed circle) for the model structure of GroEL is compared with the corresponding function obtained from the experimen-

tal data in Fig. 1b. Both the curves have one peak position at 90 Å. The maximum dimension of the simulation was a little longer than that in the experimental data. The edges of the cylinder model may be more round for GroEL molecule.

Next, we investigated if a hole perforated through the cylinder model of GroEL. If the cylinder model ($r = 68.0$ Å, $h = 150.7$ Å) has a hole of which radius is 2/5 or one third of the cylinder radius as reported by Langer et al. [7], the R_g of each model is calculated to be 68.9 or 68.2 Å that is larger than a cylinder model (66.2 Å). The patterns of $P(r)$ function of them were apparently not identical with experimental data (data not shown). If the radius of the cylinder was changed to 64 Å and the radius of the hole was kept one third of radius of this cylinder, the R_g was calculated to be 66.2 Å. The second peak of this scattering curve, however, became quite large and was not coincident with the peak of the experimental curve (Fig. 4a (i)). The peak position and the maximum dimension shown by the $P(r)$ function (Fig. 4b (i)) were in agreement with those of the cylinder model (Fig. 1b). The $P(r)$ function showed a little diminution in a region below the peak position (< 90 Å). When a minimum hole ($r = 7$ Å) through the cylinder was assumed, the R_g was estimated to be 66.4 Å. The second trough of the scattering curve was shifted to right (Fig. 4a (ii)). There was no difference between the $P(r)$ function of the minimum hole model and that of the cylinder model without the hole (Fig. 4b (ii)). These findings suggest that there is no central hole penetrating through the molecule in the cylinder model of GroEL. By the electron microscopic studies, Braig and co-workers showed that both tops of GroEL were furnished with caves that did not perforate through GroEL and suggested that the caves might play a significant role in folding process of proteins [20,21]. We made a model that had the caves on both ends of the cylinder. The radius of the cave was one third of the cylinder radius and the depth of the cave was one third of the cylinder height as was estimated by Braig and co-workers. The R_g of this model was found to be 66.9 Å. Thus, the depth of the cave was changed to one sixth of the cylinder height. The R_g was evaluated to be 66.0 Å and the scattering pattern (Fig. 4a (iii)) and $P(r)$ function (Fig. 4b (iii)) were very similar to those of the cylinder model.

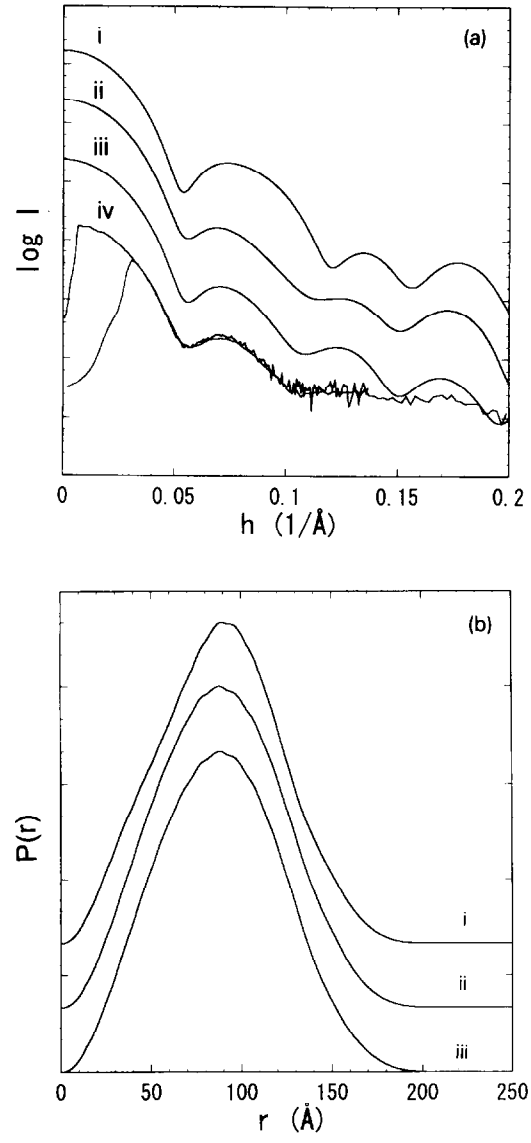

Fig. 4. (a) The X-ray scattering curves of various GroEL cylinder models as described in the text calculated by using the multi-sphere model. i: With a central hole through the molecule; the radius and height of the cylinder; 64.0 and 150.7 Å, respectively and a hole radius of 21 Å (1426 unit spheres). ii: With a central hole through the molecule, the radius and height of the cylinder; 68.0 and 150.7 Å, respectively and a hole radius 7 Å (1744 unit spheres). iii: With a cave on each top side; the radius and height of the cylinder 68.0 and 150.7 Å, respectively and a radius and height of cave, 23 and 26.0 Å, respectively (1632 unit spheres). iv: The X-ray scattering curve of 1.2% GroEL. The vertical axis is arbitrary unit. (b) The $P(r)$ functions corresponding to the various models as described above.

Finally, we have simulated the structure that shows 7-fold symmetry, consists of two heptameric rings that are stacked on each other, and has a cave on each side [20,21]. Seven grooves around the GroEL structure has a wedge shape (Fig. 5b). The angle of the wedge is 38.4°. A side-view of the heptameric ring shows a semicircle with a radius identical to the half height of the ring at both sides (Fig. 5c). The R_g of the best fit model among the structures examined was evaluated to be 66.0 Å. The maximum radius of the heptamer in the model was 76 Å and the height of the whole molecule was 150.7 Å. There is a cave on the top of the each heptamer instead of a penetrating hole. The cave of this model (two-heptameric-ring model) has a radius of 30 Å and a depth of 20 Å (Fig. 5). The scattering pattern of this model was found to be in close agreement with the experimental data (Fig. 6a). The $P(r)$ function of this model (Fig.

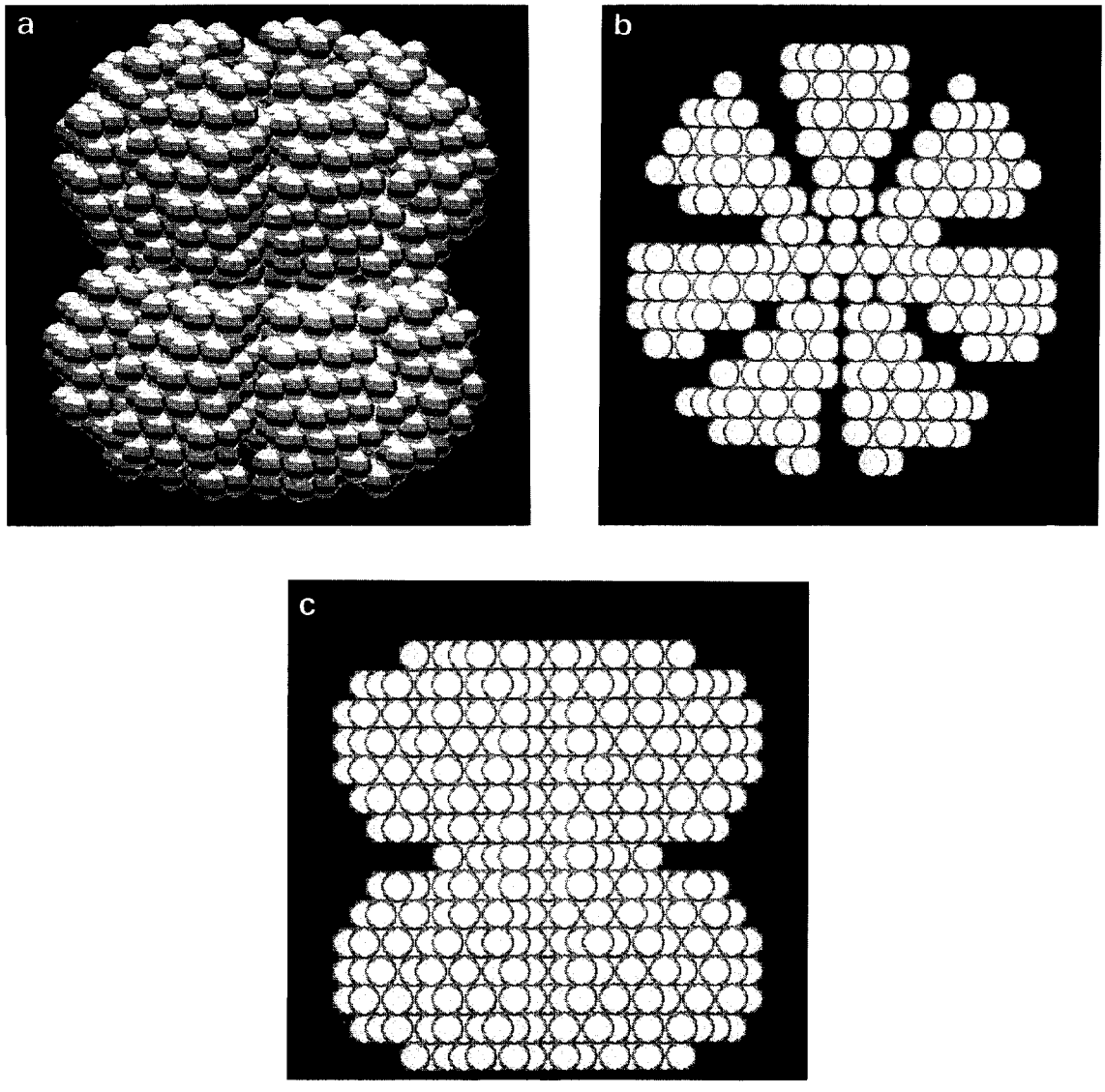

Fig. 5. The two-heptameric-ring model structure of GroEL illustrated by the multi-sphere model (1248 unit spheres). (a) Bird's eye view and (b) top view, (c) side view.

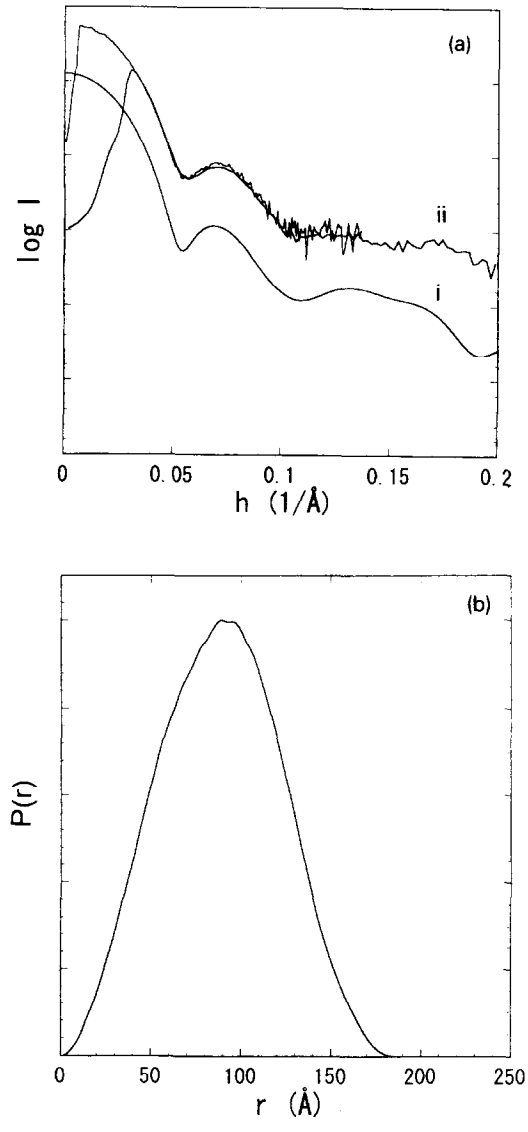

Fig. 6. (a) The X-ray scattering curves of (i) the two-heptameric-ring model as described in the text calculated by using multi-sphere model and (ii) the X-ray scattering curve at 1.2% GroEL. The vertical axis is arbitrary unit. (b) The $P(r)$ function of the two-heptameric-ring model.

6b) was nearly identical to the $P(r)$ function of the cylinder model that has a cave on each top of the cylinder(Fig. 4b (iii)). Considering the reported electron microscopic images [7] that have suggested four-ring stacked shape for GroEL instead of the double toroidal rings, we also simulated the scattering pattern of the fourfold toroidal structure and compared the scattering pattern with that for the other structures. The dimension of this model was as follows; the radius of toroidal ring was 74 Å, the height of the model was 150.7 Å and the radius and the depth of cave were 20 Å and 30 Å, respectively. The scattering pattern of this model was found to be similar to the pattern of the double toroidal model described above. We thus selected the double toroidal model of Fig. 5 because the number of parameters was less than the fourfold toroidal model. Recently, Saibil et al. [22] proposed a double toroidal model for GroEL of *Rhodobacter sphaeriodes* by electron microscopy. The scattering curves calculated from the cylinder and two-heptameric-ring models show significant differences at $h > 0.14$ Å^{-1}. However, it is difficult to judge which model fits better, as S/N ratio is not sufficient to distinguish two models at $h > 0.14$ Å^{-1}.

The structural information about the oligomeric state of GroEL has so far been limited to the electron microscopic studies. In order to understand the molecular mechanism of chaperonin action in solution, however, it is necessary to use other methods, for example, X-ray crystallography. The three-dimensional structure of GroEL is insufficiently available now [9]. Thus, we used the solution X-ray scattering that is a convenient method to elucidate the structure in solution [8,15,17,19]. The cylinder model and the two-heptameric-ring model were found to be most suitable for native GroEL. The model structures, however, do not have a penetrating hole through the molecule, which was claimed to be found in the electron microscopy studies [7,23,24].

Acknowledgements

This work has been performed under the approval of the Photon Factory Program Advisory Committee (Proposal No. 93G048). We thank Professor K. Ito for providing us the plasmid pKY206. We are indebted to Dr. G. Semisotonov for his contribution at a preliminary stage of this study. Thanks are also due to Dr. Y. Amemiya and Dr. K. Wakabayashi for adjustment of BL15A beam line.

References

[1] S.M. Hemmingsen, C. Woolford, S.M. van der Vies, K. Tilly, D.T. Dennis, C.P. Georgopoulos, R.W. Hendrix and R.J. Ellis, Nature, 333 (1988) 330.
[2] J. Martin, T. Langer, R. Boteva, A. Schramel, A.L. Horwich and F.U. Hartl, Nature, 352 (1991) 36.
[3] E.S. Bochkareva, N.M. Lissin, G.C. Flynn, J.E. Rothman and A.S. Girshovich, J. Biol. Chem., 267 (1992) 6796.
[4] R.W. Hendrix, J. Mol. Biol., 129 (1979) 375.
[5] T. Hohn, B. Hohn, A. Engel, M. Wurtz and P.R. Smith, J. Mol. Biol., 129 (1979) 359.
[6] R. Zahn, J.R. Harris, G. Pfeifer, A. Plückthun and W. Baumeister, J. Mol. Biol., 229 (1993) 579.
[7] T. Langer, G. Pfeifer, J. Martin, W. Baumeister and F.U. Hartl, EMBO J., 11 (1992) 4757.
[8] O. Glatter and O. Kratky, in O. Glatter and O. Kratky (Editors), Small Angle X-Ray Scattering, Academic Press, New York, 1982, p. 119.
[9] M.D. Spangfort, B.P. Surin, J.E. Oppentocht, C. Weibull, E. Carlemalm, N.E. Dixon and L.A. Svensson, FEBS Lett., 320 (1993)160.
[10] K. Ito and Y. Akiyama, Mol. Microbiol., 5 (1991) 2243.
[11] M.T. Fisher, Biochemistry, 31 (1992) 3955.
[12] T. Mizobata, Y. Akiyama, K. Ito, N. Yomoto and Y. Kawata, J. Biol. Chem., 267 (1992) 17773.
[13] P.A. Lanzetta, L.J. Alvarez, P.S. Reinach and O.A. Candia, Anal. Biochem., 100 (1979) 95.
[14] U.K. Laemmli, Nature, 227 (1970) 680.
[15] K. Kimura, Y. Igarashi, A. Kajita, Z.X. Wang, H. Tsuruta, Y. Amemiya and H. Kihara, Biophys. Chem., 38 (1990) 23.
[16] Y. Amemiya, K. Wakabayashi, T. Hamanaka, T. Wakabayashi, T. Matsushita and H. Hashizume, Nucl. Instrum. Methods, 208 (1983) 471.
[17] S.J. Perkins and H. Weiss, J. Mol. Biol., 168 (1983) 847.
[18] S.J. Perkins, A.S. Nealis, B.J. Sutton and A. Feinstein, J. Mol. Biol., 221 (1991) 1345.
[19] T. Igarashi, M. Sato, Y. Katsube, K. Takio, T. Tanaka, M. Nakanishi and Y. Arata, Biochemistry, 29 (1990) 5727.
[20] K. Braig, M. Simon, F. Furuya, J.F. Hainfeld and A. Horwich, Proc. Natl. Acad. Sci. USA, 90 (1993) 3978.
[21] J. Martin, M. Mayhew T. Langer and F.U. Hartl, Nature, 366 (1993) 228.
[22] H.R. Saibil, D. Zheng, A.M. Roseman, A.S. Hunter, G.M.F. Watson, S. Chen, A. Mauer, B.P. O'Hara, S.P. Wood, N.H. Mann, L.K. Barnett and R.J. Eills Curr. Biol., 3 (1993) 265.
[23] E.G. Hutchinson, W. Tichelaar, G. Hofhaus, H. Weiss and K.R. Leonard, EMBO J., 8 (1989) 1485.
[24] P. Zwickl, G. Pfeifer, F. Lottspeich, B. Dahlmann and W. Baumeister, J. Struct. Biol., 103 (1990) 197.